Technical note: Determining Arctic Ocean cold halocline and cold halostad layer depths based on vertical stability

Enrico P. Metzner[1] and Marc Salzmann[1]

[1]Institute for Meteorology, Universität Leipzig, Leipzig, Germany,

Correspondence: Enrico P. Metzner (enrico.metzner@uni-leipzig.de)

Abstract. The Arctic Ocean cold halocline layer (CHL) separates the cold surface mixed layer (SML) from the underlying warm Atlantic water, and thus provides a precondition for sea ice formation. Here, we introduce a new method in which the CHL base depth is diagnosed from vertical stability and compare it to two existing methods. Vertical stability directly affects vertical mixing and heat exchange. When applied to measurements from ice-tethered profilers, ships, and moorings, the new method for estimating the CHL base depth provides robust results with few artifacts. Comparatively large differences between our new method and two existing methods for detecting the CHL base depth were found in regions which are most prone to a CHL retreat in a warming climate. CHL base depth exhibits a seasonal cycle with a maximum depth in winter and also spring, when the SML depth is also at its maximum, but the amplitude of the CHL base depth's seasonal cycle is lower than for the SML for all three methods as expected. We also propose a novel method for detecting the cold halostad layer and study the seasonal cycle employing conservative assumptions to avoid a misclassification (including a lower bound of 50 m for the thickness). Detection of a cold halostad layer was largely confined to the Canada Basin and to the regions off the eastern coast of Greenland and also Svalbard.

1 Introduction

The Arctic Ocean outside the main Atlantic warm water inflow and the shallow marginal shelf seas is usually stratified into the cold and fresh surface mixed layer (SML), which is from ∼5 to >100 m thick, depending on region and season (Peralta-Ferriz and Woodgate, 2015), the cold halocline layer (CHL) below the SML with a base depth ∼40 to >200 m (Fig. 4 of Polyakov et al., 2018), and a layer of warm and saline Atlantic water below the CHL centered near 300 to 500 m (Aagaard et al., 1981). The CHL is also a pycnocline as density is more influenced by salinity than temperature if the temperature is low (Aagaard et al., 1981; Roquet et al., 2022). Therefore, the CHL insulates the SML from the warm Atlantic water (Aagaard et al., 1981; Lind et al., 2016; Polyakov et al., 2017, 2020). But a retreat of the CHL leads to increased vertical mixing as observed and described by Steele and Boyd (1998); Björk et al. (2002); Polyakov et al. (2017). This retreat of the CHL has been interpreted as a key feature of the increasing atlantification of the Arctic Ocean (Polyakov et al., 2017). Future climate model projections for a high emission scenario also showed increasing atlantification with warm Atlantic water reaching the surface mixed layer more frequently, especially during the cold season. This increasing atlantification in combination with sea ice loss resulted in

25 further increased annual mean upward net surface energy fluxes outside the Central Arctic along the main warm water inflow pathways (Metzner et al., 2020).

The CHL is characterized by a strong salinity gradient while temperature stays near the freezing point of sea water. Only a small proportion of the CHL is formed due to convection of brine during sea ice formation (Rudels et al., 1996; Alkire et al., 2017). Most of it is mixed and transformed water advected into the Arctic Basin from the shelves (Aagaard et al., 1981; Steele
30 et al., 1995; Mu et al., 2017). The properties of halocline water and the vertical hydrographic structures are mostly studied locally from separated observations near shelves (Lien and Trofimov, 2013; Janout et al., 2017; Baumann et al., 2018) or by models of varying complexity (Jensen et al., 2016; Metzner et al., 2020). A notable exception is the study by Polyakov et al. (2018), who derived a map of the Arctic CHL base depth based on observations.

Several methods have been proposed for identifying the CHL based on observations. Steele et al. (1995) identified cold
35 halocline water based on conditions for salinity ($34 < S < 34.5$ in the practical salinity scale) and temperature ($T < -0.5$°C). Rudels et al. (1996) defined the boundaries of the CHL by using the 34.3 isohaline. Bourgain and Gascard (2011) used a density ratio threshold to define the base of the CHL. This density ratio method was adopted among others by Polyakov et al. (2017, 2018) and Metzner et al. (2020). The density ratio is the ratio of temperature and salinity contributions to the vertical stability. A large density ratio implies that the vertical stratification is dominated by temperature and a small density ratio
40 implies that stratification is dominated by salinity. The density ratio threshold suggested by Bourgain and Gascard (2011) assumes that oceanic layers above the CHL base are almost entirely salt-stratified with temperature contributing less than 5% to the total stratification (Polyakov et al., 2018).

Bertosio et al. (2020) and Bertosio et al. (2022) distinguished between an upper and a lower CHL. Using tracer observations in the western Eurasian Basin, Bertosio et al. (2020) found the base of the lower CHL to be located at a density of
45 1027.85 kg m^{-3}. Analyzing salinity and temperature observations from the Makarov Basin and along the East Siberian continental slope, Bertosio et al. (2022) again defined the base of the upper and the lower CHL based on density thresholds and compared the results obtained with these definitions to those obtained with other definitions from the literature.

Another fairly simple and robust method for computing the CHL base depth was proposed by Metzner et al. (2020). In this method, the base of the CHL is determined by a temperature difference of 1 K between water potential temperature and
50 its freezing temperature. This temperature difference method is very sensitive to warming from below, while the density-ratio method of Bourgain and Gascard (2011) is very sensitive to the salinity profile. One drawback of the temperature difference method is a potential dependence of the optimal threshold value on region (Metzner et al., 2020).

Polyakov et al. (2018) proposed an indicator of the potential of the Arctic CHL to prevent vertical mixing based on available potential energy, adapting the density ratio threshold of Bourgain and Gascard (2011) to identify the CHL base. Here, we define
55 the CHL base based on vertical stability, motivated by the argument that vertical stability is more directly related to vertical mixing than either density, temperature, or the density ratio.

In the western Arctic, the CHL splits into an upper CHL and a lower CHL. In between lies water of Pacific origin entering the Arctic Ocean via the Bering Strait. This Pacific water is characterized by lower salinity than Atlantic water, but significantly higher salinity than fresh Arctic surface water (Lin et al., 2021). This leads to an intermediate layer called cold halostad layer

60 (Shimada et al., 2005). Similarly, interaction between glacial melt water and Arctic water north east of Greenland forms an intermediate layer of semi-saline water with low salinity gradient which is also called a cold halostad (Dmitrenko et al., 2017).

Consistent and robust descriptions of the CHL and cold halostad layer boundaries are important to understand the evolution of the structure of the upper Arctic ocean in the past and the future. Here, we propose new diagnostics for the CHL base and the cold halostad layer boundaries and compare our results for the CHL base to the result from two previously suggested methods.

65 The observational datasets on which our analysis is based are introduced in Sect. 2.1. Details of the density ratio (DR) method by Bourgain and Gascard (2011), the temperature difference (TD) method by Metzner et al. (2020), and the new stability (ST) method are provided in Sect. 2.2. The top of the CHL is assumed to coincide with the base of the SML (see Sect. 2.2). We use the kriging method to produce continuous maps of CHL and cold halostad layer boundaries (as explained in Sect. 2.3). Results are discussed in Sect. 3.

70 ## 2 Materials and Methods

2.1 Data and preprocessing

In this study, temperature and salinity observations were taken from the ice tethered profiler (ITP) project (Krishfield et al., 2008; Toole et al., 2011) and the Unified Database for Arctic and Subarctic Hydrography (UDASH, Behrendt et al., 2018). The ITPs measured temperature, salinity, and pressure twice a day while drifting with the ice floe they were tethered to. ITPs

75 deployed in the Arctic Ocean before 2018 were used here. Level III data was binned to two-day intervals in order to reduce noise and to reduce the number of missing columns in favor of a continuous time series. From the UDASH data set, only profiles, for which both temperature and salinity were available, were analyzed here. Of this subset of profiles, all profiles were used, which start closer to the surface than 5 m in order to obtain a stable estimate for the SML. The UDASH data set contains data from ships, ice-tethered profilers, profiling floats and other platforms (Behrendt et al., 2018).

80 Our analysis was limited to profiles that reach at least a depth of 500 m except in shallower regions, where the condition was that the profiles must reach down to 90% of the ocean bottom depth. This choice addresses the issue of potential sampling biases due to limited vertical extend of the observed profiles. Bathymetry data was taken from the General Bathymetric Chart of the Oceans (GEBCO) dataset (GEBCO Bathymetric Compilation Group 2021, 2021). This resulted in 116814 (pairs of) temperature and salinity profiles whose locations are shown in Fig. 1. Most measurements are concentrated in the Barents Sea

85 and only few were taken in the Central Arctic during winter. For the East Siberian Sea and the interior of the Laptev Sea, no data was available for winter and spring. Salinity was given in the practical salinity scale.

For profiles, for which only depth was reported, pressure was computed iteratively based on temperature, salinity and depth as in Metzner et al. (2020). For profiles, for which only pressure was reported, depth was computed. All values were regridded to the same vertical high-resolution grid with 0.5 m resolution in the first 50 m of the upper ocean and 1 m resolution down

90 to 200 m depth, and 2 m between 200 and 400 m depth. Below this, the resolution decreased to 2.5 m at 772.5 m depth. This results in 500 vertical grid points. After regridding, a Gaussian filter with a standard deviation of 5 m and a truncation at ±15 m was applied. When using thresholds to estimate the SML or CHL base depth, variables were linearly interpolated between two
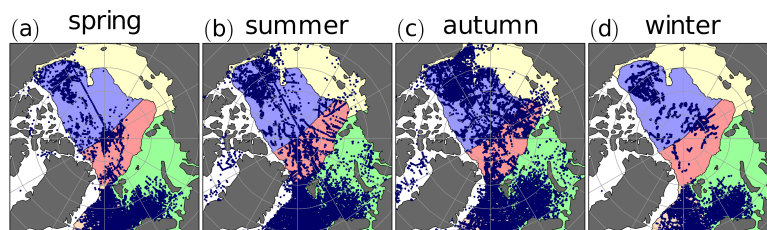
Figure 1. Map of data locations of observations for each season. Background is separated into similar regions as in the UDASH dataset Behrendt et al. (2018): Amerasian Basin (light blue), Eurasian Basin (light red), Barents Sea (light green), Shelf regions (light yellow), North Atlantic (orange) and Canadian Shelf (white).

adjacent depths. Consequently, the SML or CHL base can be located between two vertical grid points and the SML and CHL base depths do not necessarily have to coincide with the depths of the grid points.

2.2 Determining the vertical structure

2.2.1 SML depth estimate

The SML depth was estimated by a change in potential density of $0.125\,\mathrm{kg\,m^{-3}}$ as in Polyakov et al. (2017). In cases, in which a CHL is detected, the depth of the SML corresponds to the top of the CHL.

2.2.2 Base depth estimate by the density ratio (DR) method

The base of the CHL was estimated with three different methods. The first method (Bourgain and Gascard, 2011) uses the density ratio $R_\rho = (\alpha\nabla_z\theta_{\mathrm{pot}})/(\beta\nabla_z S)$ with potential temperature θ_{pot} in K, salinity S in the practical salinity scale and depth z in m. $\alpha = \rho^{-1}(\partial\rho/\partial\theta_{\mathrm{pot}})$ and $\beta = \rho^{-1}(\partial\rho/\partial S)$ are the thermal expansion coefficient and the haline contraction coefficient, respectively. Bourgain and Gascard (2011) empirically estimated that searching downward for the depth, in which R_ρ exceeds 0.05, provides a reasonable estimate for the base of the CHL. The density ratio represents the slope in the temperature(θ)-salinity(S) diagram scaled by α and β and is a proxy for the transition between a halocline and a thermocline. This method will subsequently be referred to as the density ratio (DR) method.

2.2.3 CHL base depth estimate by the temperature difference (TD) method

The second method (Metzner et al., 2020) uses the difference ΔT between the ocean temperature θ and the sea water freezing temperature T_{freeze}. The freezing temperature was calculated from Gill (1982). The base of the CHL was calculated as the depth, in which ΔT first exceeds $1\,\mathrm{K}$. This threshold was estimated to be high enough, that the "cold" core of the CHL is detectable, and low enough to separate the CHL from the Atlantic water with core temperature approximately $1.5\,°\mathrm{C}$ to $3\,°\mathrm{C}$ ($T_{\mathrm{freeze}} \approx -2\,°\mathrm{C}$ leads to $\Delta T \approx 3.5\,°\mathrm{C}$ to $5\,°\mathrm{C}$ at the core). In cases in which the temperature threshold was first exceeded in a

depth smaller than $80\,\mathrm{m}$, the search was continued $0.5\,\mathrm{m}$ below this depth. This method will be referred to as the temperature difference (TD) method.

2.2.4   CHL base depth estimate by the stability (ST) method

The third method uses the local vertical stability as parameter, which is directly linked to vertical mixing. The stability was computed from $L = \log_{10}(N^2)$, where $N = \sqrt{-(g/\rho)\,(\partial\rho/\partial z)}$ is the Brunt-Väisälä-frequency. The stability threshold is based on the density ratio threshold $R_\rho = 0.05$. It was derived from the following relationship:

$$\rho^{-1}\nabla_z\rho = \beta\nabla_z S - \alpha\nabla_z\theta_{\mathrm{pot}} = \beta\nabla_z S\,(1 - R_\rho) \tag{1}$$

With stable $\beta = (7.82 \pm 0.03)\cdot 10^{-4}$ over a wide range of temperature, salinity and pressure values ($-1.2\ldots 2.0\,^{\circ}\mathrm{C}$, $32\ldots 37$, $50\ldots 350\,\mathrm{dbar}$) and the salinity gradient in m^{-1}:

$$L = \log_{10}(-\nabla_z S) - 2.137 \pm 0.002 \tag{2}$$

Expecting the salinity gradient to be around $0.01\,\mathrm{m}^{-1}$, the resulting stability threshold should be $L \approx -4.14$.

This threshold is searched from $600\,\mathrm{m}$ or at the lowest point (at least $500\,\mathrm{m}$ deep outside the shallower regions according to the conditions for including profiles in the analyses described above) to the surface, as no CHL base was observed deeper than that and stability is mostly decreasing with depth below the CHL and SML. Seldom, the first estimate is in warm water (detected by $\Delta T > 2\,\mathrm{K}$, doubled DT-threshold for safety) due to measurement uncertainties in the temperature and salinity profiles. In such cases, a second search for the stability threshold is started slightly above. When the maximum stability is lower than the threshold, which can happen in shallow regions, the temperature difference ΔT at the base of the SML was checked against the threshold from the TDmethod. If ΔT is greater than $2\,\mathrm{K}$, the water mass was considered Atlantic water and the CHL thickness was set to zero. Otherwise, the algorithm failed and a fill value was returned. This method will be further referred to as stability (ST) method.

2.2.5   Halostad boundary estimates

In case of multiple stability maxima in the vertical profile, the thickness and the depth of the cold halostad are estimated. The cold halostad separates the CHL into an upper and a lower branch. It is associated with a stability minimum between two stability maxima. In order to estimate the thickness of the cold halostad, we first compute the mean of the stability minimum and the stability maximum associated with the lower branch of the CHL. This value is used to define the boundaries of the cold halostad. The depth of the cold halostad is estimated as the mean of the upper and lower bound. A cold halostad will only be recognized by the algorithm if the vertical distance between deeper stability maximum the first upper occurrence of that same stability value is at least $50\,\mathrm{m}$, and this stability layer has at least a relative depth of 0.2 in $\log_{10}(\mathrm{N}^2)$. In rare cases, in which more than one layer fulfills these conditions, only the lowest of these layers is identified as a cold halostad.

2.2.6 Occurrence frequency of the CHL and cold halostad

Occurrence frequencies of the CHL were computed for each method individually based on whether the criteria for estimating the CHL base depth were satisfied. Furthermore, a lower threshold of $0.001\,\mathrm{m}$ was used for the CHL thickness, below which
145   no distinctive layer is assumed to exist. Cases in which either the criteria was not satisfied or else the thickness was computed to be less than $0.001\,\mathrm{m}$ were the classified as "no CHL". This includes cases in which the CHL and the SML bottom coincide within numerical accuracy and cases in which we initially computed a value for the CHL base depth that was smaller than the value for SML base depth.

The depth of the cold halostad layer was computed whenever data was available and the conditions for identifying a cold
150   halostad layer as described above were fulfilled. The occurrence frequency for the cold halostad layer was only computed for a region in the Canada Basin. Outside this Canada Basin region, the occurrence frequency was not computed due to the sparsity of observations in these regions.

2.3 Kriging

The estimates of the SML thickness, the CHL base depth and the occurrence frequency of the CHL are inter- and extrapolated
155   with kriging. Kriging (e.g. Deutsch, 1994) is a tool from geostatistics for interpolation, extrapolation and smoothing at locations without direct measurements by data from surrounding observations. Those observations are weighted together depending on the local variability estimated by a multidimensional autocovariance function. The latter is approximated with a so called semi-variogram model. In this analysis only the spherical semi-variogram model is used (Mert and Dag, 2017; Reshid, 2019). The weights take into account the clustering of the observations as it uses the inverse of the correlation-distance matrix between
160   input points and the correlation-distance vector between input points and the point of interest. All inter-/extrapolation weights are calculated from the location and distribution of given information without prior knowledge of ocean currents.

Here, kriging was performed on an azimuthal-equidistant projection. The North Pole was used as the central reference point. $0°\,\mathrm{E}$, $90°\,\mathrm{E}$, $180°\,\mathrm{E}$ and $90°\,\mathrm{W}$ are on negative y-axis, positive x-axis, positive y-axis and negative x-axis respectively. The resolution is $0.46875°$ or roughly $52\,\mathrm{km}$ at the North Pole. The year was equally separated into 12 periods to simplify
165   calculations and time averaging afterwards. This lead to $36\mathrm{x}12 = 432$ time steps and a temporal resolution of about $30.4\,\mathrm{days}$.

Each quantity was prepared for kriging in three steps:

1. A spatial trend of the time mean was computed.

2. Outliers were removed for each season separately. Data values were identified as outliers if the difference to the spatial trend was lower (higher) than the $25^{\mathrm{th}}(75^{\mathrm{th}})$ percentile decreased (increased) by 1.5 times the inter quartile range.

170   3. The spatial trend was subtracted from the raw data. The resulting anomalies were normalized to ensure a nearly constant variance for the entire Arctic.

After kriging, the results were rescaled back to local variance and the spatial trend was added to retrieve the original local value range. Removing outliers and subtracting spatial trends are common practice in kriging. The code, which was used in this study, is available on GitHub with version v0.0.5 from http://doi.org/10.5281/zenodo.7572759.

3 Results

3.1 CHL base depth

In Figure 2, we compare three different methods for determining the CHL base depth for ITP 74. Starting from the Laptev Sea in October 2012, ITP 74 drifted across the Central Arctic, almost reaching the East Greenland Sea. Until May 2014, there is evidence of a well-defined and stably stratified CHL separating the less stably stratified Atlantic water from the SML. In May 2014, the SML deepens and the CHL disappears, as previously noted by Polyakov et al. (2017). After July, the situation becomes less clear. The stability at about 80 m depth remains low, possibly pointing at the residual of a mixed layer well below the diagnosed SML base. Below this layer, warm Atlantic water is found (Fig. 2b, compare also figure 3b of Polyakov et al., 2017). The origin of the fairly stable intermediate layer centered at about 20 m is less clear.

The CHL base depth as diagnosed by the DR and the ST method agree well until May 2014. Both methods trace the pronounced stability gradient at the CHL base (Fig. 2d). The TD method, which is less sensitive to the salinity gradient by design, instead traces the temperature gradient in Fig. 2b and places the CHL base about 20 m below the base as identified by the DR and the ST method. Neither the ST nor the TD method show spurious depth minima reaching the SML for this particular ITP.

During the final months, when the SML is diagnosed to be rather shallow, the DR method diagnoses a somewhat thicker CHL compared to the ST method. The TD method again traces the temperature gradient in Fig. 2b. The CHL base diagnosed with the DR method during the final months is ∼20 m below that diagnosed by Polyakov et al. (2017) using the same method and the same input data, albeit without prior temporal averaging and vertical smoothing. Before the deepening of the SML in May 2014, the CHL base depth from the DR method agrees well with Polyakov et al. (2017), except noise. On the one hand, binning the data in to two-day intervals results in a smoother CHL base compared to figure 3 of Polyakov et al. (2017). On the other hand, spurious depth minima still occur. As in Polyakov et al. (2017) and Metzner et al. (2020), such spurious minima can reach all the way to the SML. Spurious minima are also found for other ITPs, but not for all ITPs. Furthermore, not only the DR method but also the TD method occasionally yields spurious minima (Supplement 1, see also discussion of Fig. 3 below). However, for the model data analyzed in Metzner et al. (2020), warm Atlantic water was indeed often found directly underneath the SML during halocline thinning events. Artifacts such as the spurious CHL base depth minima found in Fig. 2 for the DR method are nevertheless a reason for concern.

Figure 3 shows profiles of temperature, salinity, Turner angle, and stability sorted by the CHL base depth from the DR, the TD, and the ST method in a 3° radius around 74°N 145.5°W in the Beaufort Sea. Cases in which the criteria for detecting the CHL were not met were excluded. This resulted in a different number of profiles for each method. Included in Fig. 3 are, however, cases in which the base depth of the CHL was set to the SML depth because the CHL base was diagnosed to either be
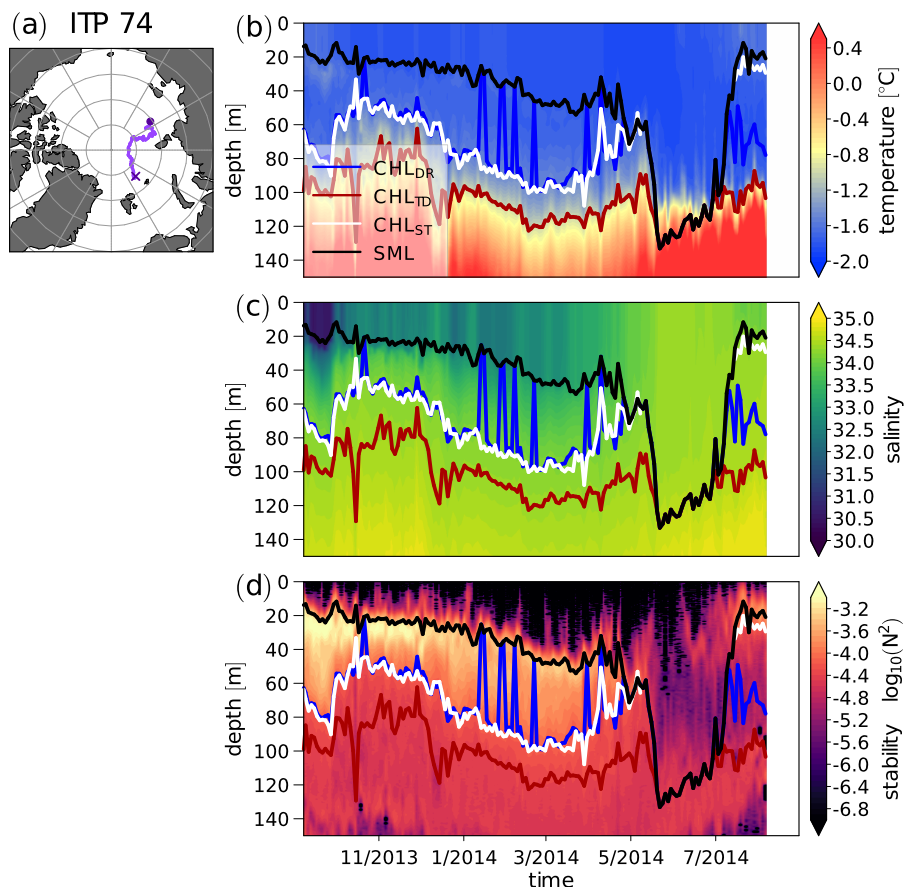
Figure 2. Location of measurements (a) and timeseries of (a) temperature, (b) salinity, and (c) vertical stability along the path of ITP 74. The circle and the cross in (a) mark the beginning and the end of the ITP 74 track, respectively. The colored lines in (b–d) are the base of the SML (black) and the CHL base depths derived by the DR method (blue), the TD method (red) and the ST method (white). Salinity is given in the practical salinity scale.

above the SML base or coincided with the SML base to within 0.001 m, and which are otherwise also classified as "no CHL". The latter is rather often the case for the DR method, as evidenced by the numerous points in the upper left part of Fig. 3b where the SML and CHL_{DR} base depth coincide. In between, there are many cases in which the CHL_{DR} base is located less than 30 m below the SML base, as evidenced be the numerous almost vertical lines in the upper right corner of Fig. 3b. For the first few hundred profiles in Fig. 3b, a cold and stable layer (CHL) that separates the mixed layer from the warmer water below is found underneath the line indicating the CHL base depth that was identified using the DR method (CHL_{DR}), indicating the occurrence of spurious CHL base depth minima.

The TD method also shows artifacts (Fig. 3c). But compared to the DR method, it is somewhat less prone to locating the CHL base close to the SML in the presence of clear indications of a CHL in the temperature and salinity fields. In particular,
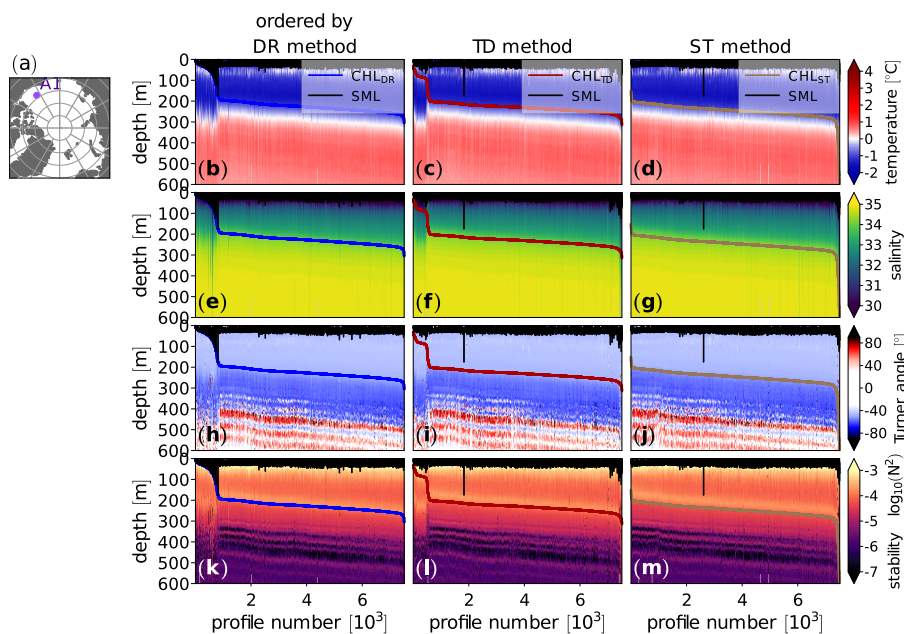
Figure 3. All used profiles of (b,c) temperature, (d,e) Turner angle and (f,g) stability profiles within 3° radius around 74° N 145.5° W (A1, shown in a) in the Beaufort Sea ordered by estimated cold halocline base depths (left CHL$_{DR}$, right CHL$_{ST}$). Lines are base depths of SML (black), cold halocline layer derived with DR method (blue), TD method (dark red) and ST method (brownish-gray).

there are nearly no cases in which the CHL$_{TD}$ base coincides with the SML base, and which would erroneously be classified as "no CHL". While none of the three methods is completely free of artifacts, the ST method (Fig. 3d) appears to perform best under these particular conditions.

3.2 CHL occurrence frequency

The occurrence frequency of the CHL is analyzed in Fig. 4. Figure 4a to c shows occurrence frequencies based on simple nearest-neighbor (NN) averaging, and Fig. 4d to f time-averaged kriging results. As expected, all three methods detect a CHL in the Arctic Basin in most cases. However, even in the basin, the DR method yields numerous isolated minima in the nearest neighbor map (Fig. 4a). The occurrence frequency in the basins in the smoothed map from the DR method (Fig. 4d) is also lower compared to the other two methods.

Overall, the CHL occurrence frequency from the DR method shows evidence of noise. On the one hand, the observations from ITP 74 in Fig. 2 suggest a rather variable CHL base depth in the parts of the Central Arctic on the way towards the East Greenland Sea. On the other hand, Figure 3 and Supplement 1 suggest that some of the "no CHL" cases in which the CHL base was above the SML base are related to spurious minima in the CHL base depth.

The potential role of spurious minima in the DR method can perhaps be best assessed by comparing the results from different methods. Because the ST and the TD method produce less artifacts while still capturing cases like the one in Fig. 2 for ITP 74,
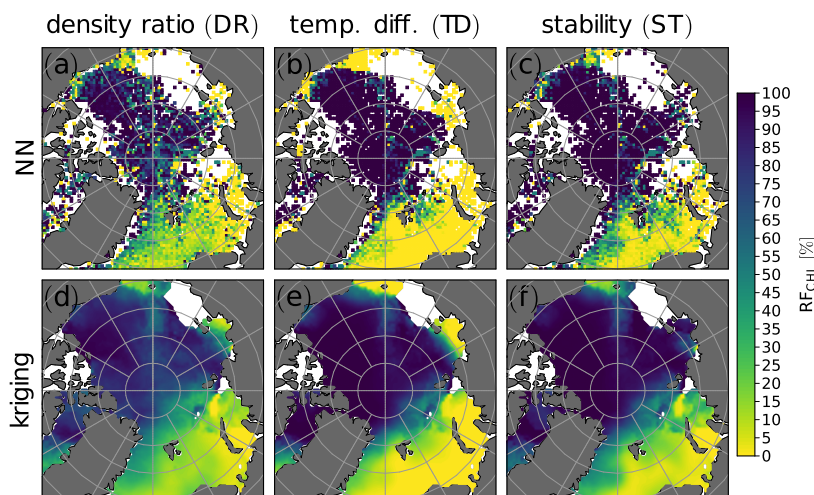
Figure 4. Map of occurrence frequency of cold halocline derived by (a,d) density-ratio algorithm, (b,e) temperature-difference algorithm and (c,f) the new stability algorithm. Those were calculated by (a-c) simple nearest-neighbor averaging and (d-f) kriging.

in which the SML deepened all the way to the Atlantic water, we deem the higher occurrence frequencies in the Arctic Basin based on the ST and the TD method more realistic compared to those based on the DR method.

The situation outside the Central Arctic is more complicated, and not surprisingly, large differences between the three methods are found in the East Greenland Sea, the Barents Sea and the Atlantic. Two of the three methods occasionally detect a CHL in the Northern Atlantic, where only the TD method shows a near zero occurrence frequency (please refer to Supplement 2 for additional discussion of this issue). In order to prevent the DR and the ST method from identifying a CHL in relatively warm water, one could either limit the region to which the method is applied or else introduce additional constraints on the water temperature.

Limiting the region is clearly a sensible choice in a stable climate. However, limiting the region to a region in which a stable CHL is found at most times limits us in studying regional shifts. With regard to shifts due to climate change, one should be aware that methods differ regarding requirements for how cold the CHL must be.

3.3 Maps of CHL boundaries

Figure 5a shows the mean base depth of the SML (top of the CHL) as identified by a change in potential density of $0.125 \, \mathrm{kg \, m^{-3}}$ based on NN-averaging. The map that results from kriging and the difference between the two maps are shown in Figures 5b and c. The annual mean SML depth in the East Siberian Sea and the interior of the Laptev Sea in Fig. 5a and b is most likely underestimated because of a lack of data in winter and spring.
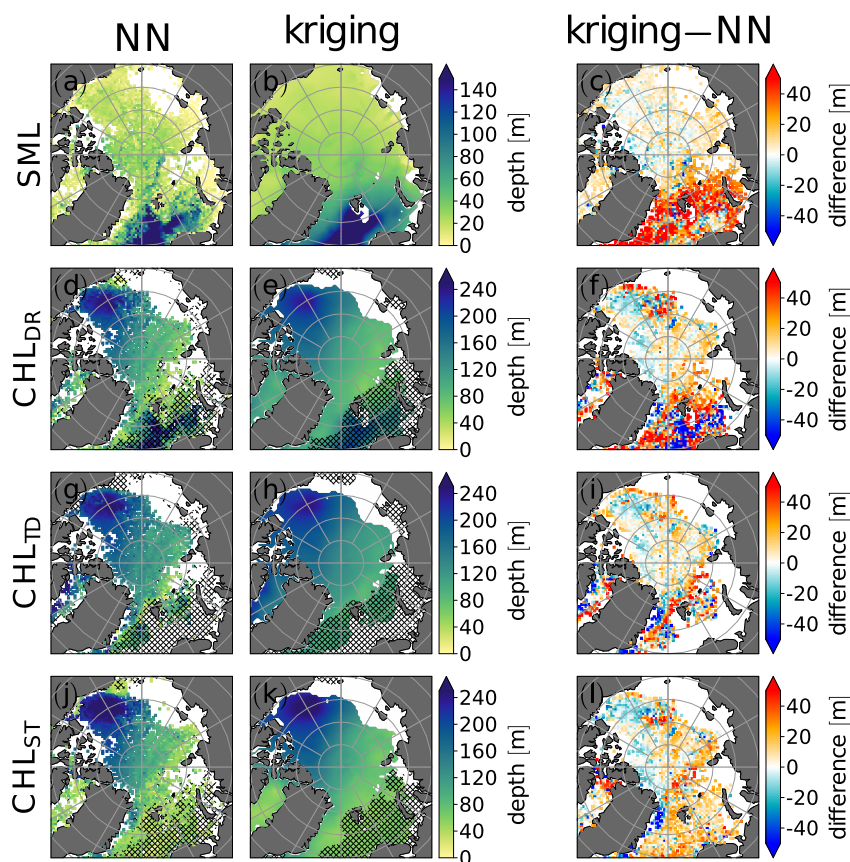
Figure 5. Comparison of (left) simple nearest-neighbor averaging to (center) kriging results with (right) difference plot for (a–c) thickness of SML and CHL base depth derived by (d–f) DR method, (g–i) TD method and (j–l) the new ST method. Points where the relative occurrence frequency of the CHL is below 1% were masked out in (d–c). Hatching indicates regions where the CHL occurrence frequency is below 25%. The SML depth in the East Siberian Sea and the interior of the Laptev Sea is based on observations in summer and fall.

245   The SML depth gradient with a comparatively deep annual mean SML in the Barents Sea, intermediate values in the Eurasian basin, and a comparatively shallow annual mean SML in the Amerasian Basin and the Chukchi Sea in Fig. 5a and b is in line with Fig. 14 of Peralta-Ferriz and Woodgate (2015).

    Although kriging acts to smooth the field, Fig. 5b still shows some small scale variability in the Central Arctic, which may result from relatively sparse observations in winter and spring (Fig. 1) in combination with a fairly pronounced seasonal cycle
250 (Fig. 6).

    The time mean CHL base depths determined from the DR method (Fig. 5d, e), the TD method (Fig. 5g, h), and the ST method (Fig. 5j, k) show a similar overall pattern. Comparatively deep time mean CHL bases below 200 m are found in the Canada Basin. The CHL base depth decreases as one moves from the Canada Basin through the central Amerasian Basin and

then across the North Pole into the Eurasian Basin. This overall pattern is consistent with figures 4g and h of Polyakov et al.

255 (2018). This CHL base depth gradient is roughly opposite to the gradient of the SML depth.

There are, however, several notable differences between the methods to determine the CHL base depth. For example, the TD method yields somewhat larger CHL base depths over the Central Arctic compared to the DR and the ST method. A particularly striking difference in Fig. 5 is found for the CHL base depth in the Barents Sea. While CHL occurrence frequencies in the Barents Sea are fairly low for all three methods, they differ notably, depending on which method is used to detect the CHL

260 base (Fig. 4). For the DR method, the CHL base depth decreases from the Barents Sea toward the Central Arctic. This contrasts the finding by Steele et al. (1995) that the CHL forms in the Barents Sea and deepens where Atlantic water sinks at the slopes north of the Barents Sea into the Eurasian Basin. On the other hand, complex situations similar to the one observed by ITP 74 are difficult to capture by methods that to some extent rely on simplification. We nevertheless chose to include the Atlantic and the Barents Sea in our comparison, in part because it helps to highlight problems, which with increasing atlantification may

265 also occur in other regions.

Furthermore, as indicated above, the CHL occurrence frequency in the Barents Sea is generally low. Especially for the TD method, a CHL is rarely detected in the Barents Sea (Fig. 4b). Because the CHL base depth is only computed for cases in which a CHL is detected, the time mean SML depth in Fig. 5 often exceeds the time mean depths of the CHL in the Atlantic and also the Barents Sea.

270 The kriged CHL base maps (Figures 5e, h, k) are smoother compared to the kriged SML map (Fig. 5b), in part because of a smaller seasonal cycle (Fig. 6). Artifacts in the DR method are partially filtered out here because spurious depth minima in the CHL base often reach the SML, so that these cases are not taken into account in computing the mean CHL base depths.

3.4 SML and CHL base depth seasonality

The seasonality of the SML and the CHL base depths are investigated in Fig. 6. Insufficient data availability is an issue

275 especially in the East Siberian Sea and the interior of the Laptev Sea, where both the seasonal cycle of the SML depth and the CHL base depth are most likely underestimated because of the absence of observations in winter and spring. The SML base depth varies more strongly with season than the CHL base depths for the East Greenland Sea, the Barents Sea, and the Atlantic. Together with the different spatial gradients in annual mean depths, this presumably makes the CHL in these regions more prone to ventilation events in winter, such as the ones investigated by Polyakov et al. (2018). This stronger seasonal cycle

280 of the SML is also generally consistent with our finding from models that CHL thinning events were most frequent in winter and spring, when the SML is deep (Metzner et al., 2020).

In the Amerasian Basin and the Chukchi Sea, the seasonal cycle of the SML depth is much smaller, often with maximum depths in March and April (Fig. 6u). The CHL base depth on the other hand, shows a seasonal cycle also near the Chukchi Shelf in the Canada Basin (e.g. Fig. 6h,l,p, and t), which could be an effect of Pacific water entering through the Bering Strait.

285 In parts of the East Siberian Sea, the maximum SML thickness is reached in autumn (Fig. 6u), but this is probably an artifact due to insufficient data availability.
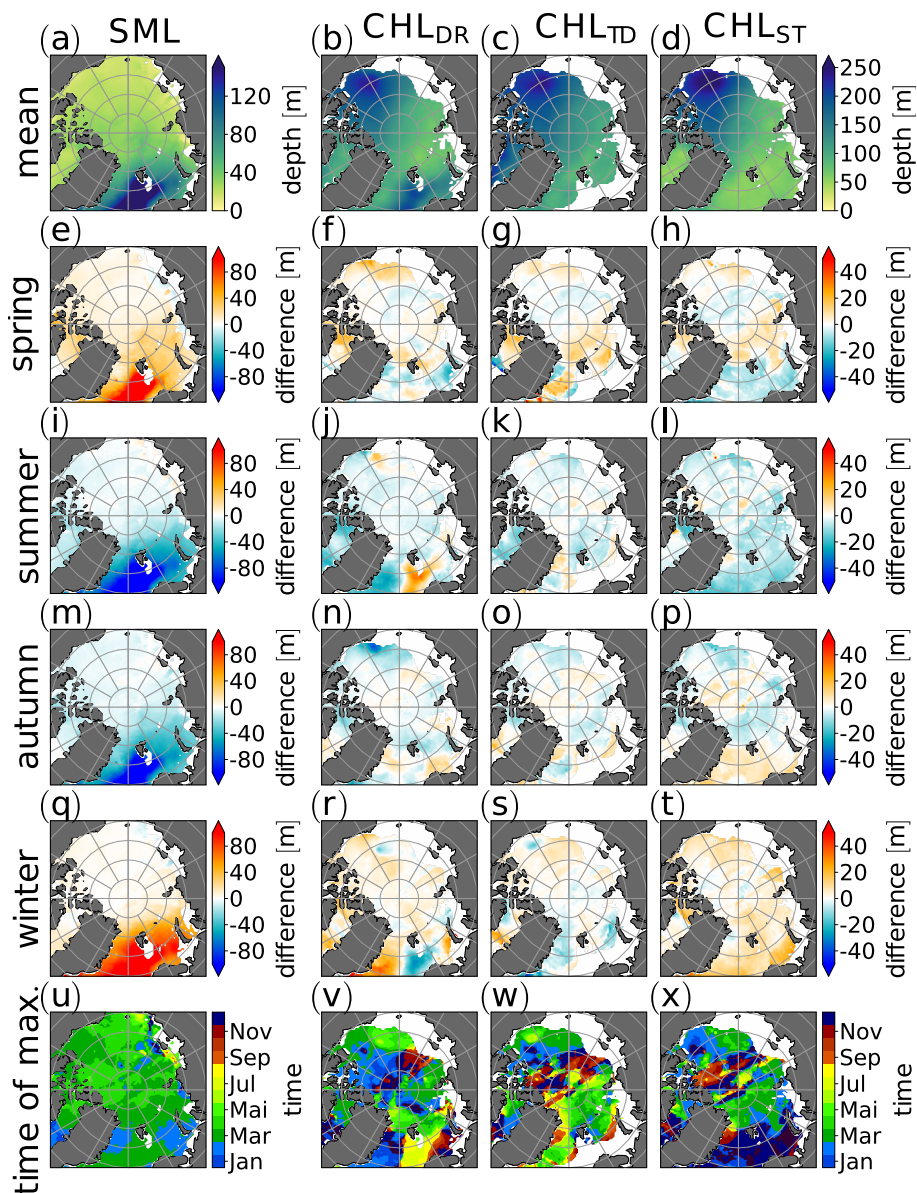
Figure 6. Annnual mean of (a) SML depth, CHL base depth derived by (b) the density-ratio method, (c) the temperature-difference method, and (d) the new stability method. The corresponding seasonal means are shown in (e) to (f). The phase of the seasonal cycle in (u) to (x) is estimated via a cosine fit.

Differences between methods in CHL base depth for the individual seasons occur mainly in regions in which also the CHL occurrence/detection frequency varied. This again warrants a note of caution when applying these methods in the regions which
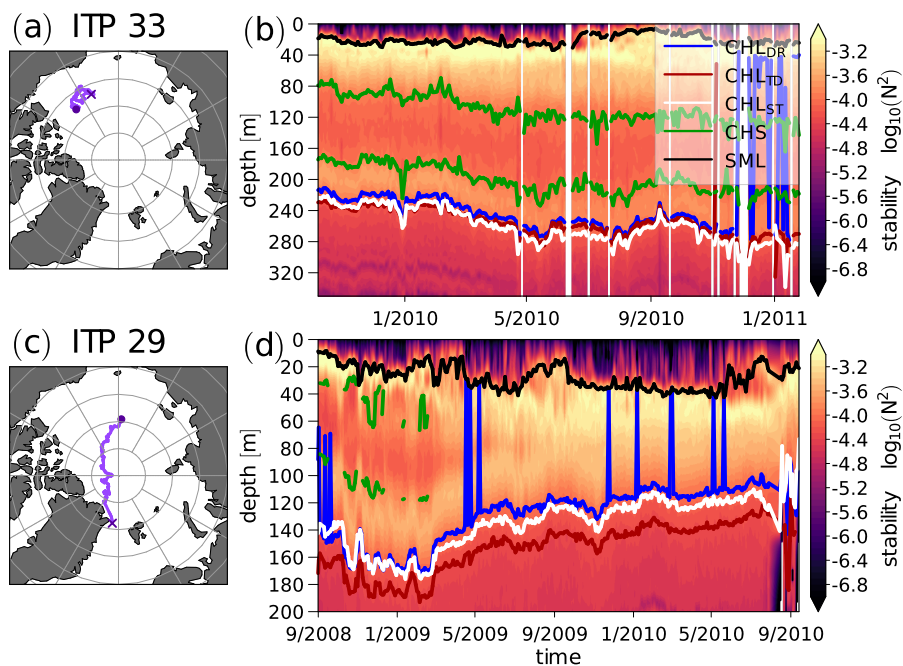
Figure 7. Same as Fig. 2a and d for (top) ITP 33 and (base) ITP 29. Additionally, the results of the cold halostad bound estimation are shown in dark green.

are most prone to changes in the CHL occurrence frequency. Outside these regions, the seasonal cycle of the CHL base depth

290   is largely consistent across the methods.

For example, in winter, the CHL base depths increases almost across the entire Arctic. Only the TD method shows moderate decreases in the East Greenland Sea and north of the Barents Sea. A reason for the decrease might be that the TD method is more prone to not detecting any CHL at all in winter either because the SML base is below the CHL base that would otherwise have been detected or else because the condition on the water temperature is not met. For the cases in which a CHL is detected,

295   it is shallower. Furthermore, because of the kriging, regions with near-zero CHL occurrence frequency can be more strongly affected by neighboring regions.

3.5   Estimation of cold halostad boundaries

In the Canada Basin, the CHL structure is more complex and features an upper layer and a lower layer (Shimada et al., 2005). This is for example reflected by the bimodal vertical stability profile in Fig. 7 along the track of ITP 33. The new algorithm

300   described in Sect. 2.2 was designed to provide estimates for the location of the cold halostad layer, which lies between these two halocline layers. The top and base depth timeseries derived with the new algorithm are shown by dark green lines (Fig. 7). At the moment the algorithm is designed to avoid misclassifications of the cold halostad by requiring the vertical extent of the 'stability valley' to be (a) at least 0.2 orders of the squared Brunt-Väisälä-frequency and (b) to be greater than 50 m. This
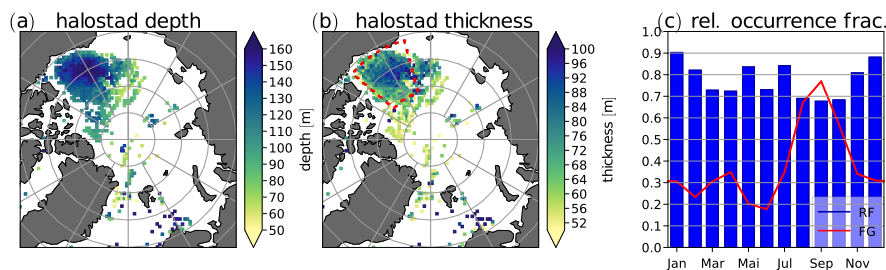
14

Figure 8. Map of mean (a) depth and (b) thickness of derived cold halostad. (c) Monthly relative occurrence fraction (RF, blue bars) of the cold halostad in the Canada Basin region (area enclosed by red dashed lines in (b) and fraction of grid points (FG) for which at least one observation was available in the respective month (red line).

leads (a) to breaks in the cold halostad boundary lines visible for ITP 29 in Fig. 7 and (b) to shallow halostad layers not being detected.

Collecting all available observations with detected cold halostad bounds per grid cell leads to the map of the cold halostad shown in Fig. 8. The main occurrence region of the cold halostad is the Canada Basin, where Pacific water circulates between the SML and Atlantic water (Shimada et al., 2005). Employing conservative assumptions to avoid a misclassification (including a lower bound of 50 m for the thickness), we detect a cold halostad layer in the Canada Basin ~70-90% of the time, except in August, September, and October when the occurrence frequency is slightly below 70%. In August, September, and October the fraction of grid points for which observations were available within the Canada Basin was also particularly high. Therefore, more points at the edge of the Canada Basin region in region in Fig. 8b, where the occurrence frequencies decrease, may have been included in the analysis. Furthermore, a cold halostad was detected near the coasts of Greenland where glacial cold water acts similar to the Pacific semi-saline water (Dmitrenko et al., 2017).

4 Summary and discussion

We introduced a new method for determining the CHL base depth based on vertical stability, compared it to two existing methods, and combined two existing comprehensive observational datasets to study the upper layers of the Arctic Ocean, generating maps of SML depth, CHL base depth, and also cold halocline depth and thickness for cases in which the cold halostad is thicker than 50 m and an additional requirement for the vertical extent of the stability minimum is fulfilled.

Unlike the two existing methods, the new method to detect the CHL base yielded few artificial CHL base depth minima. A particularly striking difference between the new method and the two existing methods was found in the Barents Sea. For the DR method, the CHL base depth decreased from the Barents Sea toward the Central Arctic. This contrasts the finding by Steele et al. (1995) that the CHL forms in the Barents Sea and deepens where Atlantic water sinks at the slopes north of the Barents Sea into the Eurasian Basin.

325 The lack of a requirement for water temperature in the DR and the new ST method was found to be problematic as one approaches the Atlantic and may be problematic when applying these methods in a warmer climate. Although an additional constraint on the water temperature could be applied in combination with the DR and the ST method in order to decrease the number of false CHL detections in comparatively warm water, it would come at the cost of decreasing the sensitivity to the vertical salinity gradient. The problem of detecting a CHL base in comparatively warm water is altogether avoided by the TD

330 method, which is highly sensitive to warming from below, but not directly (or only implicitly) to changes in salinity.

Because differences between the methods to detect the CHL bottom exist, one should always strive to ensure that the outcome from such methods is consistent with the raw data and beware of limitations in different regions. Unfortunately, our study suggests that the results from different methods to determine the CHL base depth tended to differ most in those regions in which the CHL was expected to be most affected by current climate change. Better understanding the properties of different

335 methods can help to choose between more and less appropriate methods, based on the specific scientific question.

We also suggested a method that attempts to identify the cold halostad based on stability. To our knowledge, this is the first time that such a method has been devised and applied to a comprehensive dataset. Because we found it necessary to introduce constraints on the cold halostad thickness and the depth of the stability minimum, our method suffers from a low detection sensitivity and altogether misses cold halostad layers that are thinner than $50\,\mathrm{m}$. Nevertheless, a cold halostad was frequently

340 detected in the Canadian basin throughout the year.

One method to advance cold halostad and CHL detection in the future may lie in the application of artificial intelligence. This would require a-priori manual classification applied to a training and an evaluation dataset. In the absence of objective criteria that work under most circumstances, such manual classification would ultimately have to rely on expert judgment, which may in turn introduce a different set of problems. Given the various shortcomings of traditional threshold methods,

345 AI-based methods could nevertheless be useful.

Author contributions. E.P.M. devised the new method for determining the Arctic Ocean cold halocline and cold halostad layer depths and performed the data analysis. Both authors contributed equally to writing the manuscript.

Competing interests. The authors declare that they have no conflict of interest.

References

360   Aagaard, K., Coachman, L. K., and Carmack, E.: On the halocline of the Arctic Ocean, Deep Sea Res. Part I Oceanogr. Res. Pap., 28, 529–545, https://doi.org/10.1016/0198-0149(81)90115-1, 1981.

Alkire, M. B., Polyakov, I., Rember, R., Pnyushkov, A., Ivanov, V., and Ashik, I.: Combining physical and geochemical methods to investigate lower halocline water formation and modification along the Siberian continental slope, Ocean Sci., 13, 983–995, https://doi.org/10.5194/os-13-983-2017, 2017.

365   Baumann, T. M., Polyakov, I. V., Pnyushkov, A. V., Rember, R., Ivanov, V. V., Alkire, M. B., Goszczko, I., and Carmack, E. C.: On the seasonal cycles observed at the continental slope of the eastern Eurasian Basin of the Arctic Ocean, J. Phys. Oceanogr., 48, 1451–1470, https://doi.org/10.1175/JPO-D-17-0163.1, 2018.

Behrendt, A., Sumata, H., Rabe, B., and Schauer, U.: UDASH – Unified Database for Arctic and Subarctic Hydrography, Earth Syst. Sci. Data, 10, 1119–1138, https://doi.org/10.5194/essd-10-1119-2018, 2018.

370   Bertosio, C., Provost, C., Sennéchael, N., Artana, C., Athanase, M., Boles, E., Lellouche, J.-M., and Garric, G.: The western Eurasian Basin halocline in 2017: Insights from autonomous NO measurements and the Mercator Physical System, J. Geophys. Res. Oceans, 125, e2020JC016 204, https://doi.org/10.1029/2020JC016204, 2020.

Bertosio, C., Provost, C., Athanase, M., Sennéchael, N., Garric, G., Lellouche, J.-M., Kim, J.-H., Cho, K.-H., and Park, T.: Changes in Arctic halocline waters along the East Siberian Slope and in the Makarov Basin from 2007 to 2020, J. Geophys. Res. Oceans, 127,
375   https://doi.org/10.1029/2021jc018082, 2022.

Björk, G., Söderkvist, J., Winsor, P., Nikolopoulos, A., and Steele, M.: Return of the cold halocline layer to the Amundsen Basin of the Arctic Ocean: Implication for the sea ice mass balance, Geophys. Res. Lett., 29, 1–8, https://doi.org/10.1029/2001GL014157, 2002.

Bourgain, P. and Gascard, J. C.: The Arctic Ocean halocline and its interannual variability from 1997 to 2008, Deep Sea Res. Part I Oceanogr. Res. Pap., 58, 745–756, https://doi.org/10.1016/j.dsr.2011.05.001, 2011.

380   Deutsch, C. V.: Kriging with strings of data, Math. Geol., 26, 623–638, https://doi.org/10.1007/BF02089245, 1994.

Dmitrenko, I. A., Kirillov, S. A., Rudels, B., Babb, D. G., Pedersen, L. T., Rysgaard, S., Kristoffersen, Y., and Barber, D. G.: Arctic Ocean outflow and glacier–ocean interactions modify water over the Wandel Sea shelf (northeastern Greenland), Ocean Sci., 13, 1045–1060, https://doi.org/10.5194/os-13-1045-2017, 2017.

GEBCO Bathymetric Compilation Group 2021: The GEBCO_2021 grid - a continuous terrain model of the global oceans and land.,
385   https://doi.org/10.5285/c6612cbe-50b3-0cff-e053-6c86abc09f8f, 2021.

Gill, A. E.: Atmosphere-ocean dynamics (International Geophysics Series, Volume 30), Academic Press, 1982.

Janout, M. A., Hölemann, J., Timokhov, L., Gutjahr, O., and Heinemann, G.: Circulation in the northwest Laptev Sea in the eastern Arctic Ocean: Crossroads between Siberian River water, Atlantic water and polynya-formed dense water, J. Geophys. Res. Oceans, 122, 6630–6647, https://doi.org/https://doi.org/10.1002/2017JC013159, 2017.

390   Jensen, M. F., Nilsson, J., and Nisancioglu, K. H.: The interaction between sea ice and salinity-dominated ocean circulation: implications for halocline stability and rapid changes of sea ice cover, Clim. Dyn., 47, 3301–3317, https://doi.org/10.1007/s00382-016-3027-5, 2016.

Krishfield, R., Toole, J., Proshutinsky, A., and Timmermans, M.-L.: Automated ice-tethered profilers for seawater observations under pack ice in all seasons, J. Atmos. Ocean Technol., 25, 2091–2105, https://doi.org/10.1175/2008JTECHO587.1, 2008.

Lien, V. S. and Trofimov, A. G.: Formation of Barents Sea branch water in the north-eastern Barents Sea, Polar Res., 32,
395   https://doi.org/10.3402/polar.v32i0.18905, 2013.

Lin, P., Pickart, R. S., Våge, K., and Li, J.: Fate of Warm Pacific water in the Arctic Basin, Geophys. Res. Lett., 48, e2021GL094 693, https://doi.org/10.1029/2021GL094693, e2021GL094693 2021GL094693, 2021.

Lind, S., Ingvaldsen, R. B., and Furevik, T.: Arctic layer salinity controls heat loss from deep Atlantic layer in seasonally ice-covered areas of the Barents Sea, Geophys. Res. Lett., 43, 5233–5242, https://doi.org/10.1002/2016GL068421, 2016.

400 Mert, B. A. and Dag, A.: A computer program for practical semivariogram modelling and ordinary kriging: A case study of porosity distribution in an oil field, Open Geosci., 9, 663–674, https://doi.org/10.1515/geo-2017-0050, 2017.

Metzner, E. P., Salzmann, M., and Gerdes, R.: Arctic Ocean surface energy flux and the cold halocline in future climate projections, J. Geophys. Res. Oceans, 125, e2019JC015 554, https://doi.org/10.1029/2019JC015554, 2020.

Mu, L., Zhao, J., and Zhong, W.: Regime shift of the dominant factor for halocline depth in the Canada Basin during 1990-2008, Acta
405 Oceanol. Sin., 36, 35–43, https://doi.org/10.1007/s13131-016-0883-0, 2017.

Peralta-Ferriz, C. and Woodgate, R. A.: Seasonal and interannual variability of pan-Arctic surface mixed layer properties from 1979 to 2012 from hydrographic data, and the dominance of stratification for multiyear mixed layer depth shoaling, Prog. Oceanogr., 134, 19–53, https://doi.org/10.1016/j.pocean.2014.12.005, 2015.

Polyakov, I. V., Pnyushkov, A. V., Alkire, M. B., Ashik, I. M., Baumann, T. M., Carmack, E. C., Goszczko, I., Guthrie, J., Ivanov, V. V.,
410 Kanzow, T., Krishfield, R., Kwok, R., Sundfjord, A., Morison, J., Rember, R., and Yulin, A.: Greater role for Atlantic inflows on sea-ice loss in the Eurasian Basin of the Arctic Ocean, Science, 356, https://doi.org/10.1126/science.aai8204, 2017.

Polyakov, I. V., Pnyushkov, A. V., and Carmack, E. C.: Stability of the Arctic halocline: a new indicator of Arctic climate change, Environ. Res. Lett., 13, https://doi.org/10.1088/1748-9326/aaec1e, 2018.

Polyakov, I. V., Rippeth, T. P., Fer, I., Alkire, M. B., Baumann, T. M., Carmack, E. C., Ingvaldsen, R., Ivanov, V. V., Janout, M., Lind, S.,
415 Padman, L., Pnyushkov, A. V., and Rember, R.: Weakening of cold halocline layer exposes sea ice to oceanic heat in the eastern Arctic Ocean, J. Clim., 33, 8107–8123, https://doi.org/10.1175/JCLI-D-19-0976.1, 2020.

Reshid, T. M.: Kriging and simulation in Gaussian random fields applied to soil property interpolation, Am. J. Theor. Appl. Stat., 8, 296–305, https://doi.org/10.11648/j.ajtas.20190806.21, 2019.

Roquet, F., Ferreira, D., Caneill, R., Schlesinger, D., and Madec, G.: Unique thermal expansion properties of water key to the formation of
420 sea ice on Earth, Sci. Adv., 8, https://doi.org/10.1126/sciadv.abq0793, 2022.

Rudels, B., Anderson, L. G., and Jones, E. P.: Formation and evolution of the surface mixed layer and halocline of the Arctic Ocean, J. Geophys. Res. Oceans, 101, 8807–8821, https://doi.org/10.1029/96JC00143, 1996.

Shimada, K., Itoh, M., Nishino, S., McLoaughlin, F., Carmack, E., and Proshutinsky, A.: Halocline structure in the Canada Basin of the Arctic Ocean, Geophys. Res. Lett., 32, https://doi.org/10.1029/2004GL021358, 2005.

425 Steele, M. and Boyd, T.: Retreat of the cold halocline layer in the Arctic Ocean, J. Geophys. Res., 103, 10 419–10 435, https://doi.org/10.1029/98JC00580, 1998.

Steele, M., Morison, J., and Curtin, T.: Halocline water formation in the Barents Sea, J. Geophys. Res., 100, 881–894, 1995.

Toole, J. M., Krishfield, R. A., Timmermans, M.-L., and Proshutinsky, A.: The ice-tethered profiler: ARGO of the Arctic, Oceanography, 24, 126–135, http://www.jstor.org/stable/24861307, 2011.